CFD Research Corporation
215 Wynn Dr. • Huntsville, Alabama 35805 • Tel.: (256) 726-4800 • FAX: (256) 726-4806 • info@cfdrc.com

CFDRC

ON-CHIP TRANSPORT OF BIOLOGICAL FLUIDS IN MEMS DEVICES

Quarterly Progress Report

(November 22, 1998 – February 20, 1998)

By
M.G. Giridharan and
S. Krishnamoorthy

February 1999

CFDRC Report: 4843/7

Sponsored by
Defense Advanced Research Projects Agency
Electronics Technology Office
DARPA Order No. E994/A
Program Code No: 7S10
Issued by DARPA/CMO under Contract #MDA972-97-C-0015

1.0 PROJECT STATUS

The work on this project started on May 20, 1997. The project is currently on schedule.

2.0 DESCRIPTION OF PROGRESS

The work performed during this quarter is listed below:

(i) An Implicit Multi-dimensional Model for Electroosmosis has been developed and successfully integrated with CFD-ACE+ code.

(ii) Extension of the above-mentioned model to simulate electrophoretic flow is currently underway.

The following sections will provide detailed discussions on the activities performed during this reporting period.

3.0 AN IMPLICIT MULTI-DIMENSIONAL FINITE-VOLUME MODEL FOR ELECTROOSMOTIC FLOW

3.1 Introduction

As mentioned in the previous quarterly reports, a one-dimensional implicit finite-volume method to model electrophoresis phenomena has been developed. In the present reporting period, this model has been extended for multi-dimensional geometries to simulate electroosmotic flow in microdevices. Electrophoresis model in CFD-ACE+ will be incorporated during the next quarterly period.

3.2 Governing Equations

Mass transport of a charged specie due to electroosmosis is governed by three major mechanisms, such as diffusion, convection and electric field. To model these mechanisms, the equations governing the convection and diffusion of charged species in an electric field must be solved. The governing equations are:

Continuity Equation

$$\nabla \cdot \mathbf{V} = 0 \tag{1}$$

Momentum Equation

$$\rho\left[\frac{\partial \mathbf{V}}{\partial t} + (\mathbf{V}\cdot\nabla)\mathbf{V}\right] = -\nabla p + \mu\nabla^2\mathbf{V} + \rho_e\mathbf{E} \tag{2}$$

where $\mathbf{V}$ is the velocity vector, ρ is the density of the buffer solution, p is pressure, μ is the dynamic viscosity of the buffer, ρ_e is the electric charge density, and $\mathbf{E}$ is the electric field intensity. The electric field is related to the electric potential Φ via

$$\mathbf{E} = -\nabla\phi \tag{3}$$

The electric potential is governed by

$$\nabla^2\Phi = -(\rho_e/\varepsilon) \tag{4}$$

where ε is the electrical permittivity of the buffer solution. Substituting Eqs. (3) and (4) into (2), the momentum equation can be written as:

$$\rho\left[\frac{\partial \mathbf{V}}{\partial t} + (\mathbf{V}\cdot\nabla)\mathbf{V}\right] = -\nabla p + \mu\nabla^2\mathbf{V} + \varepsilon\left[\nabla^2\Phi\cdot\nabla\Phi\right] \tag{5}$$

In the above formulation thermal convection due to Joule heating, and chemical reactions within buffer solution have been neglected. In the electrolyte solution, positively and negatively charged ions resulting from the reactions of dissociation interact with the electric field that can be calculated from Eq. (4). On a macroscopic scale, the solution is electrically neutral. The electro-neutrality condition is violated only on scales comparable to Debye radius around each ion. This radius is usually of the order of several nanometers. Therefore, for macroscopic consideration electro-neutrality condition can be used. However, special attention should be given to regions very close to the channel wall, where a electrical double layer would exist and same charge ions concentrate in close proximity resulting in a potential called "ζ" potential. An approach used by Patankar and Hu (1998) is used to solve Eq. (4).

In electroosmotic flow, when an external electric field is applied, the charged species lying next to the wall will start moving. Thus the magnitude of the ζ potential and applied electric field determine the speed of motion. Typically when the Debye thickness is small and charge on the wall is not very significant, the distribution of ζ potential is affected very little by the applied electric field. Also, when the inertial terms are small, i.e., at very low flow velocity, the fluid motion has very little influence on charge distribution. Under these conditions, the total potential can be decomposed into two parts, ϕ, the potential due to the applied electric field and ψ, potential due to charge on the walls:

$$\Phi = \phi + \psi \tag{6}$$

Consequently, Eq. (4) can be written as two separate equations

$$\nabla^2\phi = 0 \tag{7}$$

and

$$\nabla^2\psi = -(\rho_e/\varepsilon) \tag{8}$$

The electric field that generates the force on the charged species causing electroosmotic flow is given by

$$\mathbf{E} = -\nabla\left(\phi + \psi\right) \tag{9}$$

Following Patankar and Hu (1998) and adapted from original works of Grossman and Colburn (1992), the charge density can be expressed as

$$\rho_e = -\varepsilon\kappa^2\psi \tag{10}$$

where κ is inverse of Debye thickness. The governing equations can be rewritten as:

$$\rho\left[\frac{\partial \mathbf{V}}{\partial t} + (\mathbf{V}\cdot\nabla)\mathbf{V}\right] = -\nabla p + \mu\nabla^2\mathbf{V} + \varepsilon\kappa^2\psi\nabla\phi \tag{11}$$

$$\nabla^2\phi = 0 \tag{12}$$

$$\nabla^2\psi = \kappa^2\psi \tag{13}$$

3.3 Numerical Scheme

The governing equations (Eqs. (1), (11), (12) and (13)) are first discretized in space and time using a finite-volume based methodology. An important motivation for choosing this methodology is that it has excellent conservation property that is satisfied even at the numerical level. This ensures that numerical scheme does not introduce any spurious source and sink terms. The spatial region is subdivided into individual non-overlapping computational cells whose union will reproduce the entire computational domain. This discretization is achieved using CFD-GEOM, the geometric-modeling and grid generation software developed and marketed by CFD Research Corporation. Data transfer, storage and retrieval are accomplished using CFD-DTF utility. The present model is also capable of handling arbitrary polyhedral grids such as those commonly occur in unstructured grids.

The finite volume discretization transforms the partial differential equations into a set of algebraic equations. The discretized equations are assembled into matrices and solved using iterative linear solvers. The solution methodology used in CFD-ACE+ is based on SIMPLEC (Semi-Implicit Pressure Linked Equations, Consistent) algorithm, first introduced by Van Doormal and Raithby (1984). This is derived from SIMPLE algorithm, described in detail by Patankar (1980).

3.4 Geometry

The geometry of the device used in the present study is similar to one used by Fan and Harrison (1994) and explained in detail by Patankar and Hu (1998). This is shown in Figure 1. The device is shaped like a cross-channel with the intersection of four reservoirs numbered 1 through

4. The injection of the sample solution is affected by applying a voltage between reservoirs 1 and 2. This will drive the sample from reservoir 1 to 2 (for $\phi_1 > \phi_2$ and $\zeta < 0$), across the intersection, thus creating a sample plug in the path between reservoirs 3 and 4. By applying suitable electric potential between reservoirs 3 and 4, the plug will be separated from the cross-stream and start flowing in the side channel connecting reservoirs 3 and 4. Sample separation does not occur during injection process between reservoirs 1 and 2 since the sample flows continuously. The present study is focussed on the flow patterns developed at the intersection of cross channels under different applied electric field and Reynolds number of the flow. The scalar transport equation solver for sample concentration will be implemented in the next quarter. Since the flow variations and magnitude of velocity are negligibly small in the z direction, the cross-channel is modeled as a two-dimensional geometry.

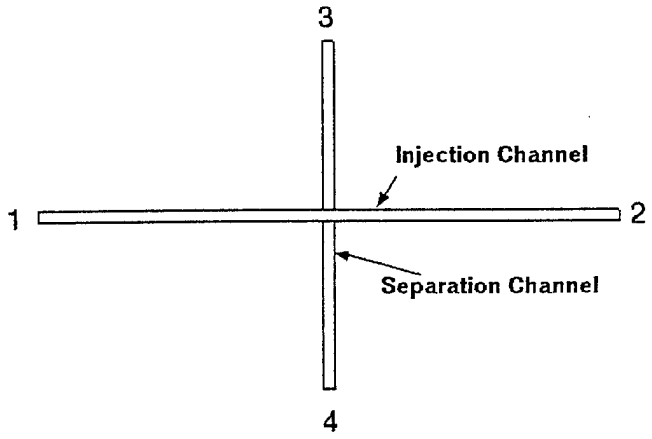

Figure 1. Cross-Channel Device

3.5 Boundary Conditions

The boundary conditions for the potential equations are the external applied voltage and ζ potential at the wall. A constant potential (ϕ_1) is applied at the reservoir 1 and reservoir 2 is grounded. The potential applied at reservoirs 3 and 4 is changed to effect electroosmotic flow and sample plug injection. The walls of the channel are assumed to be electrically insulated. A constant ζ potential (space charge potential) is applied at the wall. The driving force for the fluid motion is generated by the electric field.

3.6 Results and Discussions

The buffer solution is assumed to be very dilute:

$$\varepsilon = 6.95 \times 10^{-10}\ C^2/J.m$$

$$\zeta = 100\ Mv$$

$$\mu = 10^{-3}\ N\ s/m^2$$

$\rho = 1000\ Kg/m^3$

$\phi_1 = 150\ V$

$w = 30\ \mu m$

where w is the width of the channel. Reynolds number (Re) is defined as:

$$Re = \rho\left(\frac{\phi_1 \varepsilon \zeta}{\mu w L}\right)\left(\frac{w}{\mu}\right) \tag{13}$$

where L is the distance between reservoirs 1 and 2. The main parameters of the problem are Reynolds number Re, inverse of Debye thickness κ, potential applied at reservoirs 3 (ϕ_3) and 4 (ϕ_4), and the ratio L/w. The effects of Reynolds number and potential at side reservoirs (ϕ_3 and ϕ_4) will be analyzed. A constant potential of -100 mV is applied at the walls. This implies that the wall is negatively charged and will form a thin layer of positively charged ions next to wall. Application of positive electric field will induce a fluid velocity in the positive direction.

3.6.1 External Potential Field

Figure 2 shows the external potential field under the application of different potentials at the side reservoirs 3 and 4. Reservoir 1 is always kept at 150 V and reservoir 2 is always grounded. When the potential at the side reservoirs is 75 V, it is observed that by symmetry, potential at the center of the channel is also 75 V. As a result, there is very small variation of potential in the side channel and the electric field is almost zero. There is no net flow in these channels. Velocity vector for this case is shown in Figure 3 (a). As expected, the velocity profile is flat (plug flow).

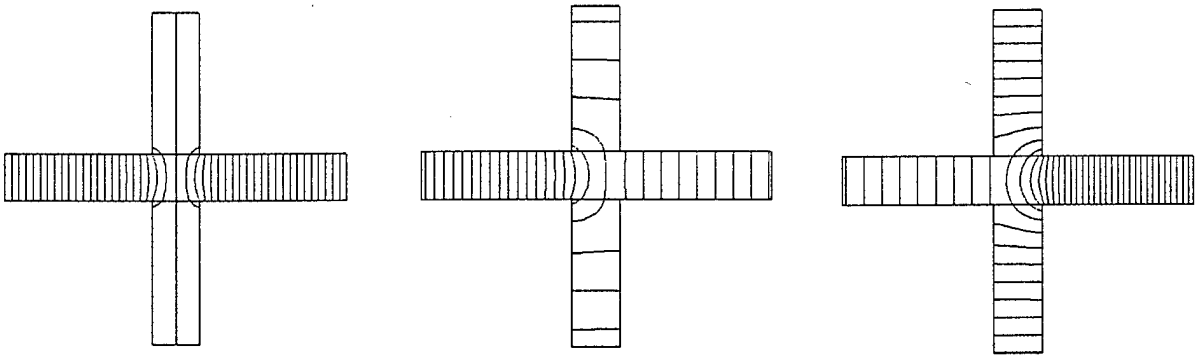

Figure 2. Contours of External Potential Field Inside Cross-Channel for Re = 1. Potential at the Side Reservoirs: (a) 75 V, (b) 37.5 V, and (c) 135 V

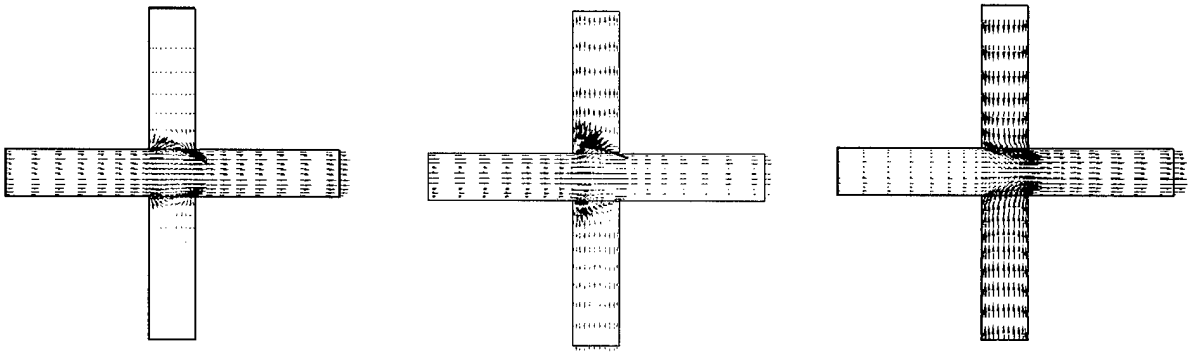

(a) (b) (c)

Figure 3. Velocity Vector Plot Inside Cross-Channel for Re = 1. Potential at the Side Reservoirs: (a) 75 V, (b) 37.5 V, and (c) 135 V. The Phenomena of Electrokinetic Focusing Can be Observed in Figure (c)

When the potential at the side reservoir is 37.5 V, the potential at the center of the channel is less than 75 V. There is also a potential gradient along the side channel and there is net flow away from the center of the channel. On the contrary, when the potential at the side reservoirs are kept at 135 V, there is a net flow towards the center of the channel. This phenomena is clearly illustrated in Figures 2(b) and (c). In Figures 3(b) and (c), the corresponding velocity vector plot is shown.

3.6.2 Potential Due to Charge on the Walls

Figure 4(a) illustrates a typical grid used in the simulation. As can be seen, the grid lines are densely packed near the wall so that variations in ζ potential due to wall charge will be resolved. In Figure 4(b), the contours of ζ potential is shown. The potential decays exponentially to zero at the center of the channel. In all the simulations shown in this report, a constant value of 1.5 μm is used as the Debye thickness.

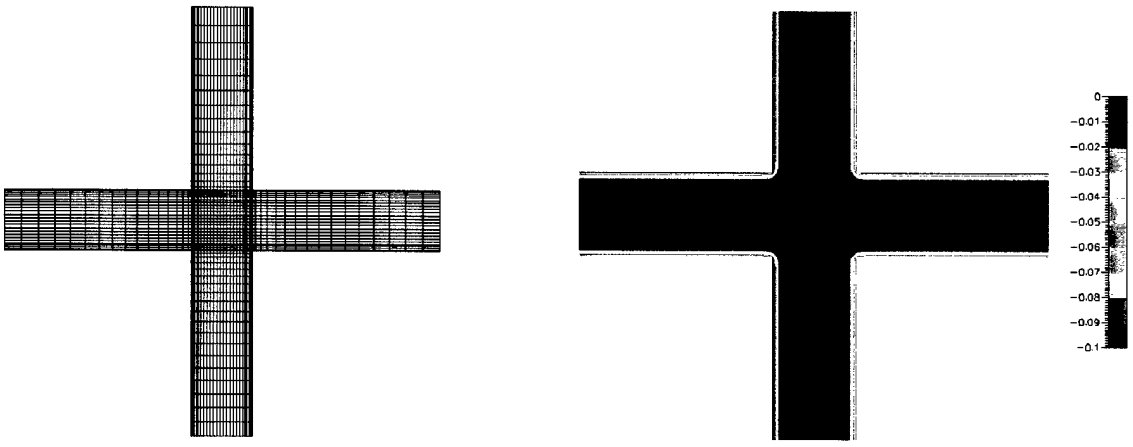

(a) (b)

Figure 4. Nonuniform Grid Used to Generate Cross-Channel Device is Shown in (a) and Contour Plots of ζ Potential is Shown in (b) for ϕ_1 = 150 V and $\phi_3 = \phi_4$ = 75 V and Re = 1

3.6.3 Effect of Reynolds Number

To understand the effect of Reynolds number on the flow field, the side reservoirs are set to a potential that is half of the potential applied at reservoir 1 (ϕ_1). This will insure that there will not be any net flow in side channels. Also, the pressure at the reservoirs is set to zero. Reynolds number is varied by changing ϕ_1. The velocity vector plot inside the injection channel is shown in Figures 5(a) and (b) for Re = 0.1 and 10, respectively. Overall it is observed that the velocity profile remains flat through out the channel except near the wall, where sharp gradients are introduced due to the imposition of noslip condition. As Re increases, velocity of flow in the injection channel increases. Consequently, the leakage of sample from the injection channel into the separation channel is reduced. This will result in more uniform sample plug.

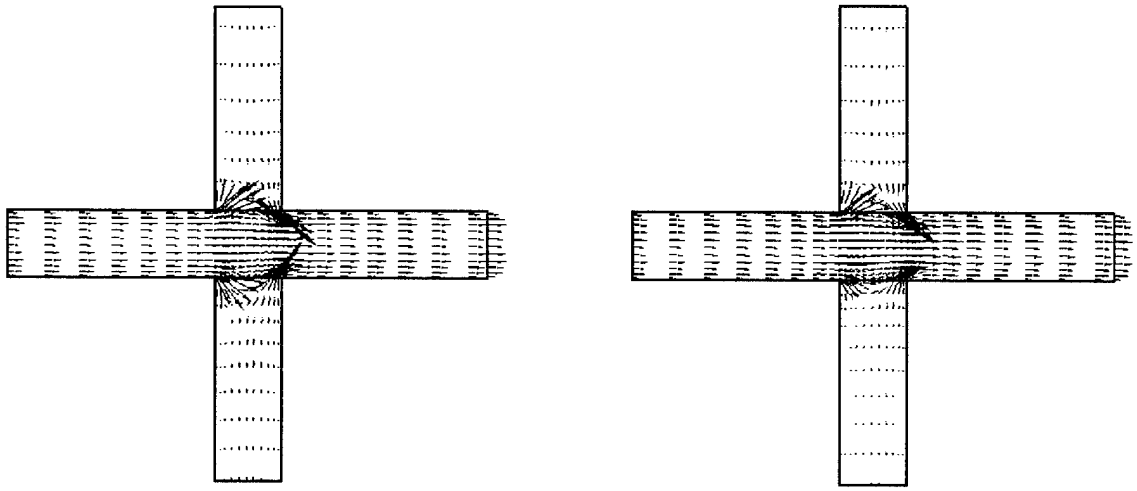

(a) (b)

Figure 5. Effect of Reynolds Number on Flow Field. The Velocity Vector Plot in Cross-Channel Device is Shown for Re = 0.1 and 10 in (a) and (b) Respectively. The Potential at Side Reservoirs is Kept at Half of ϕ_1. The Maximum Velocity Observed are 0.044 m/s and 0.24 m/s for Re = 0.1 and 10, Respectively

3.6.4 Electrokinetic Focusing

This is one way of obtaining tightly focused stream of samples at the channel intersection so that a uniformly shape sample plug may be injected into side channels for separation. This can be achieved by varying potential at the side reservoirs. For this study, Reynolds Number is set to 1.0 (ϕ_1 = 150 V) and pressure at all the reservoirs is set to zero.

As shown in Figures 2(a) and 3(a), when the potential at the side reservoir is set to 75 V, there is no net flow in side channels. When the potential is reduced below 75 V (to 37.5 V), it is observed from Figures 2(b) and 3(b) that there exists a potential gradient and fluid flow occurs from the injection channel to the separation channel. This is not desirable since it may cause the sample to leak from the injection channel and may contaminate the buffer solution. When the potential is set to 135 V, it is evident from Figures 2(c) and 3(c) that the fluid flows from the separation channel into the injection channels. The streamlines in the injection channel are squeezed at the intersection. This is desirable since the sample is restricted to remain at the

intersection. However too much squeezing can distort the shape of the plug. This technique of controlling the shape of plug by varying potential at the side channels has been used in experiments (Patankar and Hu, 1998) and computational software such as CFD-ACE+ can be used as a valuable design tool to optimize applied potential. More detailed study of this focussing will be reported in the next progress report.

4.0 PLANNED ACTIVITIES

The following activities are planned for the next quarter:

(i) Effort will be undertaken to integrate the current electrophoresis model with CFD ACE+ environment.

(ii) Multi-dimensional simulation capabilities will be developed to study of electrophoresis.

(iii) Collaborative work between CFDRC and Aclara Biosciences, InnovaTek, Biomicro Systems and Affymetrix will be pursued.

5.0 SUMMARY OF MEETINGS ATTENDED

No meeting has been attended during the reporting period

6.0 ACCOMPLISHMENTS

An implicit finite-volume based CFD model to simulate electroosmotic flow has been integrated with CFD-ACE+.

7.0 REFERENCES

1. N. A. Patankar and H. H. Hu, "Numerical Simulation of Electroosmotic Flow," Analytical Chemistry, 70 (9), pp. 1870-1881, 1998.

2. Z. H. Fan and D. Harrison, Journal of Analytical Chemistry, Vol. 66, pp. 177-184, 1994.

3. P. D. Grossman and J. Colburn, Capillary Electrophoresis, Theory and Practice, Academy Press, San Diego, 1992.

4. S. V. Patankar, Numerical Heat Transfer, Hemisphere Publishing Corporation, New York, 1980.

5. J. P. Van Doormal and G. D. Raithby, "Enhancements of the SIMPLE Method for Predicting Incompressible Fluid Flows," *Journal of Numerical Heat Transfer*, Vol. 7, pp. 147-163, 1984.

PHASE II SBIR

ON-CHIP TRANSPORT OF BIOLOGICAL FLUIDS

IN MEMS DEVICES

DARPA CONTRACT NUMBER: MDA972-97-C-0015

Total Funds	$980,000
Total Funds Used	$850,461
Estimated Cost to Complete	$129,539
Estimated Percentage of Physical Completion	$87%